ELSEVIER

Journal of Structural Geology 27 (2005) 1666–1679

JOURNAL OF STRUCTURAL GEOLOGY

www.elsevier.com/locate/jsg

Deformation of melt-bearing systems—insight from in situ grain-scale analogue experiments

Nicolas P. Walte[a,*], Paul D. Bons[b], Cees W. Passchier[a]

[a]*Tektonophysik, Institut für Geowissenschaften, Johannes Gutenberg-Universität Mainz, Germany*
[b]*Institut für Geowissenschaften, Eberhard Karls Universität Tübingen, Germany*

Received 24 June 2004; received in revised form 7 April 2005; accepted 18 May 2005
Available online 12 July 2005

Abstract

The deformation behaviour of partially molten rocks was investigated using in situ analogue experiments with norcamphor + ethanol, as well as partially molten $KNO_3 + LiNO_3$. Three general deformation regimes could be distinguished during bulk pure shear deformation. In regime I, above ca. 8–10 vol.% liquid (melt) fraction (ϕ_{bulk}), deformation is by compaction, distributed granular flow, and grain boundary sliding (GBS). At $\phi_{bulk} < 8$–10 vol.% (regime II), GBS localizes in conjugate shear zones. Liquid segregation is inefficient or even reversed as the dilatant shear zones draw in melt to locally exceed the 8–10 vol.% threshold. At even lower ϕ_{bulk} (regime III), grains form a coherent framework that deforms by grain boundary migration accommodated dislocation creep, associated with efficient segregation of remaining liquid. The transition liquid fraction between regimes I and II (ϕ_{LT}) depends mainly on the grain geometry and is therefore comparable in both analogue systems. The transition liquid fraction between regimes II and III ($\phi_{GBS\text{-}L}$) varies between 4–7 vol.% for norcamphor–ethanol and ca. 1 vol.% for $KNO_3 + LiNO_3$ and depends on system specific parameters. Regime II behaviour in our experiments can explain the frequently observed small melt-bearing shear zones in partially molten rocks and in HT experiments.

Keywords: Analogue experiments; Norcamphor; Magma segregation; Granular flow; Partially molten rocks; Grain boundary sliding

1. Introduction

Liquid-bearing systems range from almost complete solid grain aggregates with minor amounts of liquid between grains to almost fully liquid magma in which isolated crystals are suspended. The amount of liquid is one of the primary parameters that determines the rheological behaviour of such composite systems. Three main types of behaviour can be distinguished:

1. High liquid fraction: crystals are suspended in the liquid. The mechanical behaviour is controlled primarily by the liquid viscosity and can be described as that of a dilute suspension (Einstein, 1906; Ryerson et al., 1988).
2. Intermediate liquid fraction: crystals form an aggregate and the rheological behaviour is that of granular flow and grain boundary sliding (Rutter, 1997; Petford and Koenders, 1998; Paterson, 2001).
3. Low liquid fraction: grains form an interlocking load-bearing framework and the mechanics of the composite system are controlled by the rheology of the solid phase as follows (Arzi, 1978; Vigneresse et al., 1996):
   (a) The composite system is controlled by the (non-linear) viscosity of the solid, which deforms by diffusion or dislocation creep mechanisms (e.g. Hirth and Kohltstedt, 1995a,b; Gleason et al., 1999; Mei et al., 2002).
   (b) Brittle deformation by intracrystalline fracturing occurs (e.g. van der Molen and Paterson, 1979; Dell'Angelo and Tullis, 1988; Rutter, 1997; Renner et al., 2000; Holyoke and Rushmer, 2002).

Significant changes in strength and liquid transport are expected when liquid-bearing systems move from one type of behaviour to another, for instance during progressive

* Corresponding author. Address: Bayerisches Geoinstitut, Universität Bayreuth, Germany.
E-mail address: nico.walte@uni-bayreuth.de (N.P. Walte).

0191-8141/$ - see front matter © 2005 Elsevier Ltd. All rights reserved.
doi:10.1016/j.jsg.2005.05.006

melting, or during crystallisation of a magma (Arzi, 1978; van der Molen and Paterson, 1979; Vigneresse et al., 1996). Most attention has been paid to the rheological transition between melt-dominated behaviour (1 + 2) and flow dominated by the solid phase rheology (3) with its associated change in viscosity over many orders of magnitude. For this transition Arzi (1978) suggested a rheologically critical melt percentage (RCMP) that marks a sharp drop in strength. The RCMP is important to several systems, such as orogenic belts that contain partially-molten zones, like the Himalayas. If these partially-molten zones exceed the RCMP, they will constitute major zones of weakness that may mechanically detach the overlying crust from the orogenic root and mantle (Schott and Schmeling, 1998; Arnold et al., 2001). Exceeding the RCMP may also cause the wholesale mobilization and diapiric ascent of partially molten rock (Weinberg and Podladchikov, 1994; Paterson and Vernon, 1995). Strong changes in rheology with changing melt fraction are also critically important for porosity waves. These are ascending zones of increased melt-bearing porosity, which are proposed as one of the mechanisms of melt ascent beneath, for example, mid-oceanic ridges (Barcilon and Richter, 1986; Scott and Stevenson, 1986; McKenzie, 1987; Kelemen et al., 1997; Holtzman et al., 2003a). Even though the background melt percentage may be well below the RCMP, the porosity waves themselves may contain enough melt to overcome the RCMP, which has to be considered for numerical models of these processes (Rabinowicz et al., 2001).

Despite the importance of the change in behaviour from melt-dominated flow to solid-phase-dominated rheology, there is still much uncertainty about the nature of this transition. Experiments have indicated either a dramatic change in rheology when the RCMP is crossed (Arzi, 1978; van der Molen and Paterson, 1979), or a gradual transition (Rutter and Neumann, 1995; Rutter, 1997; Bagdasserov and Dorfman, 1998; Renner et al., 2000; Rosenberg, 2001). High-temperature experiments on partial melts are normally restricted to measurement of stress–strain rate relationships and post-mortem analyses of the microstructure. Comparison of rheological data for different melt fractions are complicated by the fact that the melt fraction is most commonly changed by varying the temperature (e.g. Rutter and Neumann, 1995) or the water content of a sample (e.g. van der Molen and Paterson, 1979), both of which may significantly change the viscosity of the phases. The role of melt-enhanced embrittlement is also often unclear (Rutter and Neumann, 1995).

In situ analogue experiments with partially-molten rock analogues provide a different approach to investigating these problems (Means and Park, 1994; Park and Means, 1996; Bauer et al., 2000; Rosenberg and Handy, 2000, 2001; Walte et al., 2003). Instead of focussing on the measurement of rheology, analogue experiments reveal processes on the grain-scale when a melt-bearing system is deformed. This study presents two sets of analogue experiments with a single crystalline phase (norcamphor or KNO_3) plus a liquid phase with a well-constrained behaviour as a melt analogue (ethanol or KNO_3–$LiNO_3$ melt) that is easily observable in situ (Walte et al., 2003). These systems allow continuous observation of the microstructural processes and changes in deformation behaviour as a function of a varying liquid fraction within a single experiment. The experiments show the effect of the different deformation regimes on melt-segregation. They also show that the transition between the regimes is not only a function of melt percentage, but also of the strength of the solid phase, the strain rate, the melt pressure and the wetting behaviour of the melt.

2. Experiments

Two different sets of experiments were performed. In one set, norcamphor and norcamphor-saturated ethanol liquid were used as analogues for a monomineralic solid phase and melt, respectively (cf. Walte et al., 2003). Norcamphor ($C_7H_{10}O$) is an organic crystalline compound with hexagonal symmetry and crystal–plastic rheology at room temperature, which has been used as an analogue for rock-forming minerals such as quartz or olivine (Bons, 1993; Bons et al., 1993; Herweg and Handy, 1996; Bauer et al., 2000; Rosenberg and Handy, 2000, 2001; Walte et al., 2003). The ethanol permits fast diffusion of dissolved norcamphor at room temperature so that continuous surface-energy driven grain coarsening (Ostwald ripening or liquid assisted recrystallisation) takes place as in natural systems at high temperature conditions (Walte et al., 2003).

The second set of experiments was conducted with a mixture of 90–95 wt.% KNO_3 and 5–10 wt.% $LiNO_3$. These nitrates have a eutectic point at 141 °C and therefore are in the temperature range of in situ analogue experiments. The $LiNO_3$ is completely molten at the experimental temperature so that the sample consists of a single solid phase (KNO_3) plus a KNO_3–$LiNO_3$ melt phase. Nitrates such as KNO_3 are similar to carbonates, such as calcite, in both crystallography and rheological behaviour (Tungatt and Humphreys, 1981).

No quantitative measurements of melt and solid phase viscosities could be made with our experimental setup. However, the norcamphor crystals are quite weak and the KNO_3 crystals were quite strong at the experimental conditions, while the viscosity of the two liquid phases was comparable. The norcamphor–ethanol system and the partially–molten nitrates therefore represent analogues for systems with a low and high solid–liquid viscosity ratio, respectively.

Experiments were performed in a linear, Urai–Means see-through deformation apparatus (Fig. 1b), which allows for continuous observation of the sample with a microscope

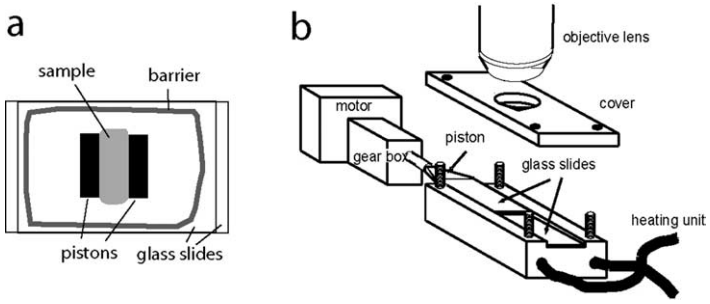

Fig. 1. (a) Setup of the sample. 100-mm-thick sample (norcamphor + ethanol or $KNO_3 + LiNO_3$) is positioned between two glass slides and surrounded by a barrier of silicone putty (only norcamphor + ethanol). (b) Sketch of the Urai–Means linear deformation apparatus. The ca. 100-μm-thick sample is situated between the glass slides.

during an experiment (Urai, 1983; Means, 1989). Approximately, 100-μm-thick samples were sandwiched between glass slides and positioned in a brass housing, which contains two heating elements and holes to view the thin-section-like sample. Pure shear deformation was induced by gluing one thin cover slip as a piston on each glass plate, on opposite sides, and sliding the upper glass plate relative to the lower one (Fig. 1a). Sliding of the glass plate was driven by a motor at a constant displacement rate, resulting in strain rates between approximately 10^{-4} and 10^{-6} s^{-1} depending on the motor used and the distance between the pistons. A barrier of silicone putty ('Rhodorsil gomme') encased the sample to inhibit evaporation of the volatile norcamphor and ethanol. At the start of the experiments, the barrier was not in contact with the sample, so that chemical interaction between the sample and the barrier was inhibited. The samples were therefore unconfined at the sides during the deformation and the liquid was free to flow into or out of the sample as a response to dilation or compaction (Fig. 1a). In long-term experiments, local dissolution and dilution of the silicone putty was observed by segregated liquid that came in contact with the putty barrier. However, no effect of the interaction between the silicone putty and the sample was noticed in the observed area. Some loss of liquid and norcamphor was only noticed in the longest lasting experiment (> 1 week).

The whole apparatus was mounted on a microscope stage to observe the microstructural evolution in the thin-section like sample. 756×512 pixel digital colour images were taken at regular intervals from 2 min to 2 h, depending on the duration of an experiment that ranged from a few hours to more than 10 days. Liquid fraction was determined by directly tracing and measuring the liquid area from the images with the image analysis software NIH image and is reported in vol.%. The precision of the area measurements and the sources of error due to image resolution are estimated to be ±0.3 vol.%. One drawback of this method is that very low liquid fractions < 1 vol.% cannot be accurately determined because individual liquid pockets can hardly be distinguished on the digital images.

3. Results

3.1. Norcamphor–Ethanol experiments

Samples were prepared by sandwiching the desired mix of fine-grained norcamphor and norcamphor-saturated ethanol directly between the glass plates and inserting the assembly into the apparatus. An effectively two-dimensional (only one layer of grains) equilibrated texture forms within a few hours of static annealing at room temperature. Grains have smoothly curved boundaries, perpendicular to the glass plates. At high (> 10 vol.%) liquid fractions, grains that are surrounded by liquid are approximately spherical in shape without crystal facets. That indicates an effectively isotropic solid–liquid surface energy of the norcamphor (Walte et al., 2003). At lower melt fractions, the grains form a foam texture, with liquid mostly located at regular triangular inward-curving grain boundary triple junctions (Fig. 2). The geometry is close to the predicted equilibrium distribution with a low solid–liquid wetting angle of about 25° (e.g. von Bargen and Waff, 1986; Laporte, 1994). However, occasional disequilibrium liquid pockets, such as larger patches or wetted grain boundaries,

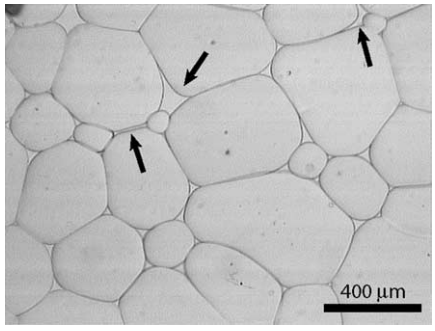

Fig. 2. Image of a statically recrystallizing norcamphor–ethanol aggregate. The grains form an equilibrated foam texture with smoothly curved grain boundaries. Liquid is situated in triangular three-grain triple junctions forming dihedral angles of approximately 25° with the norcamphor grains. Arrows point at disequilibrium features that form due to static grain growth.

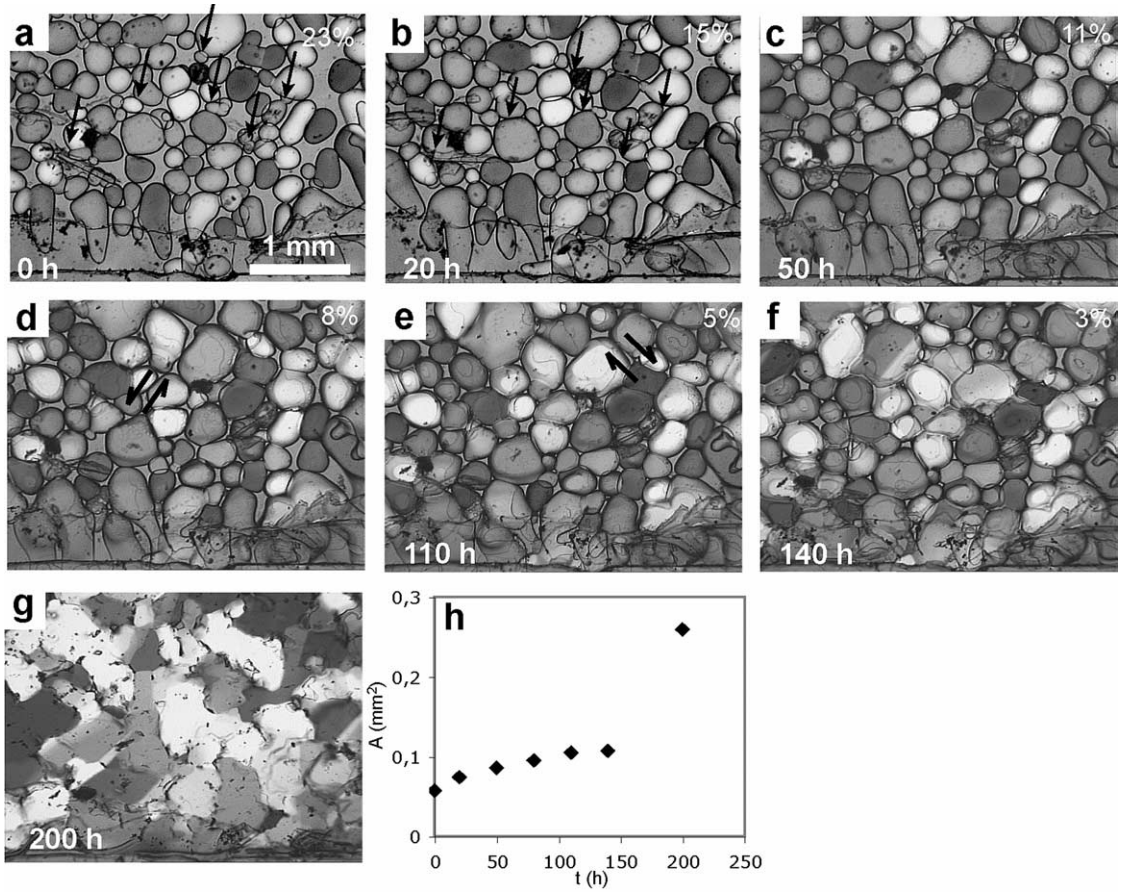

Fig. 3. Deformation of norcamphor crystals plus saturated ethanol liquid by bulk pure shear with a strain rate of $\sim 2\times10^{-6}\,s^{-1}$ (vertical shortening direction). (a) and (b) Grain coarsening accommodated compaction with minor grain boundary sliding. Arrows indicate small grains that disappear and are replaced. (c) Deformation is accommodated by granular flow. (d) and (e) Localized grain boundary sliding in small shear zones while most of the grains are already locked. (f) and (g) Locking up of grain boundaries and grain boundary migration accommodated dislocation creep. The liquid fraction at this stage is nearly zero. Images were taken with partly crossed polarizers. Bottom left numbers indicate time elapsed from the beginning of the experiment, top right numbers indicate the liquid fraction in vol.%. (h) Mean grain size versus time graph.

also occur as a result of continuous grain growth (Fig. 2) (Walte et al., 2003).

Experiments were prepared with an initially high liquid fraction of >10 vol.% (Fig. 3a). Norcamphor grains in contact with each other regularly form aggregates with welded grain boundaries (Fig. 4). This is energetically favourable for wetting angles above 0° when the ratio of solid–solid to solid–liquid surface energy is below two, so that aggregation of grains lowers the total energy of the system (e.g. Stephenson and White, 1967; Jurewicz and Watson, 1985).

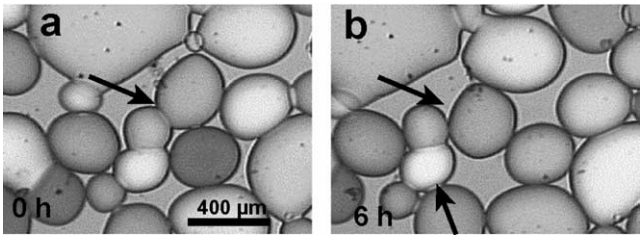

Fig. 4. Interplay of grain boundary welding and grain boundary sliding in a norcamphor + ethanol experiment at a bulk liquid fraction >10 vol.%. The aggregate in the centre is destroyed as the upper grain is sheared off (see arrows). Notice the newly formed welded boundary in the lower part of (b) (lower arrow). Images were taken with partly crossed polarizers.

Experiments were conducted with 'low' and 'high' bulk strain rates of approximately 10^{-6} and $10^{-5}\,s^{-1}$, respectively. Temperature was held constant at 30 ± 1 °C by room air conditioning, without additional heating or cooling.

During a single experiment the melt fraction always decreased within the observed area due to compaction of the sample and lateral extrusion of liquid that collected at the sides of the sample. This allowed for a continuous observation of the transition from high to low liquid-fraction behaviour.

3.1.1. 'Low' strain rate deformation

The images of Fig. 3 represent more than 8 days of deformation at a strain rate of $\sim 2\times10^{-6}\,s^{-1}$. Initially, the sample deforms by grain compaction accommodated by a

combination of grain boundary sliding-granular flow and grain coarsening (Fig. 3a and b). The grain coarsening is driven by the dissolution of small grains and simultaneous growth of large grains due to the differences in surface/volume ratio of different sized grains. This process is normally termed (liquid assisted) 'static recrystallization' or 'Ostwald ripening' (e.g. Evans et al., 2001). When a small grain disappears, a larger grain can slide into the remaining gap and occupy its space so that the static grain coarsening facilitates compaction (compare Fig. 3a and b). This mechanism, coupled with a complex grain rearrangement and minor grain boundary sliding, dominates the deformation in the beginning of the experiment. The Ostwald ripening process is responsible for slowly increasing grain size during the first 140 h of the experiment (Fig. 3h). Dissolution–precipitation processes such as 'contact melting' as reported by Means and Park (1994) were not observed and are probably of minor importance. One reason for this is the different grain shape in our experiments compared with the older experiments. It is easier for more equant grains in our samples to change position by grain boundary sliding than for the elongated grains of Means and Park (1994), so that stress concentrations are reduced. Grain boundary sliding is either distributed throughout the sample (granular flow) at a high liquid fraction exceeding ca. 8–9% or is localized in small, short-lived, often conjugate shear zones that occur at lower liquid fractions. During their activity, the shear zones have a locally stable liquid fraction as grains slide past each other (Fig. 3c–e). A shear zone can become de-activated during deformation e.g. by rotation towards the shear plane. A de-activated shear zone often compacts by redistribution of the melt in the surrounding matrix or to the edge of the sample. Welding of several grains into coherent clusters between the shear zones is another characteristic of this deformation/melt fraction stage (Figs. 3d and e and 4).

During progressive pure shear, the liquid fraction decreases slowly due to an overall compaction of the grains and lateral expulsion of liquid towards the sides of the sample. The grain-scale liquid distribution at this stage is governed by opening and closing gaps between sliding grains, by liquid redistribution due to disappearing grains, and growing grains that slide into cavities. As the grain size increases and the liquid fraction decreases, the relative effect of grain coarsening as an accommodation process for compaction decreases.

Below about 8 vol.% liquid fraction, the deformation becomes more localized into shear zones and grain boundary sliding is more and more inhibited by welded grain boundaries and the formation of larger grain clusters. Once the liquid fraction drops below 3–4 vol.%, there is a dramatic switch in microstructure and deformation mechanism (Fig. 3f and g). Grain boundary sliding is absent as all grains are locked into one single framework. The grains are now deforming internally by crystal plastic deformation, probably dislocation creep (Bons, 1993; Herweg and Handy, 1996). The grains develop undulose extinction, which regularly localizes into newly formed sub-grain boundaries usually oriented parallel to the axis of greatest compression (Fig. 5). Further rotational recrystallisation leads to the formation of new grains with high-angle boundaries (Fig. 5d).

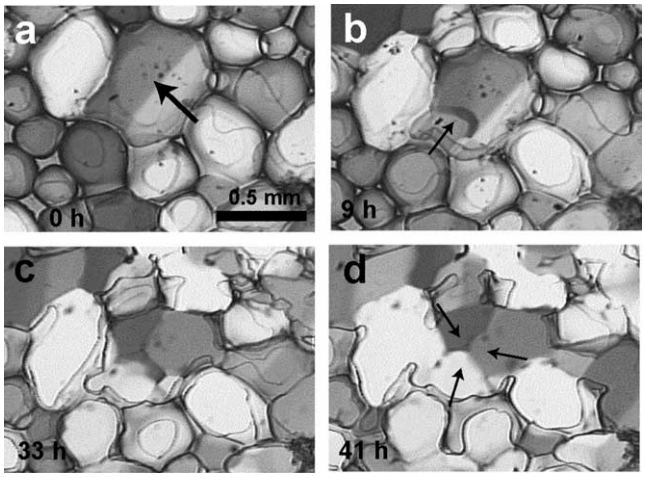

Fig. 5. Detail of the low strain rate norcamphor+ethanol experiment showing the development of a single grain (see arrow). Straight sub-grain boundary in (a) migrates slowly outwards while a new curved sub-grain boundary develops from below (b). A second sub-grain boundary develops (c) so that the grain eventually splits into three parts. The lower third becomes part of a larger bright grain. Images were taken with partly crossed polarizers. Bulk liquid fraction of (a) 2–3 vol.%.

At this stage, grain boundaries become very mobile, probably because grains are pressed against each other so that no visible liquid pockets remain between the grains. An unstable microstructure results as the grain boundaries begin to sweep other grains and become irregular and amoeboid in shape (Fig. 3g). The mean grain size increases rapidly (Fig. 3h). However, this fast grain boundary mobility is only reached once most of the liquid is expelled from the sample. As long as liquid can be observed in triple junctions and between grain boundaries, the boundaries are prevented from migrating freely. Therefore liquid patches act as a pinning phase (cf. Evans et al., 2001; Renner et al., 2002). Small remaining liquid pockets pin mobile grain boundaries for a limited time before the grain boundaries sweep over or around them and the liquid remains as round inclusions within grains (Figs. 6 and 7).

3.1.2. 'High' strain rate deformation

The deformation behaviour and microstructure in the experiments with a 'high' strain rate ($\sim 10^{-5}\,s^{-1}$) is generally similar to the 'low' strain rate behaviour described above. At a liquid fraction above ca. 8 vol.% deformation is accommodated by grain rearrangement during compaction and granular flow (Fig. 8a–c). Because of the higher strain rate, the surface energy driven grain coarsening described above is negligible as an accommodation mechanism

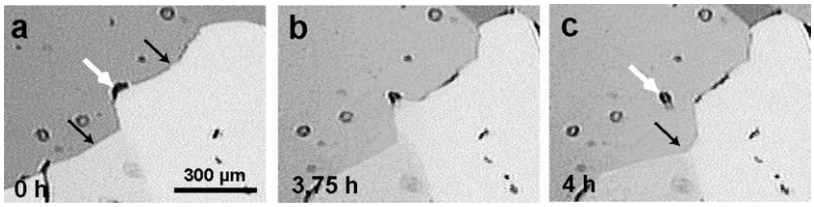

Fig. 6. 'Regular pinning' in the grain boundary migration stage of a 'low' strain rate norcamphor+ethanol experiment. (a) and (b) A moving grain boundary (arrows) is pinned by a small liquid bubble. (c) Eventually, the boundary detaches and leaves a round liquid inclusion (arrow). Images were taken with partly crossed polarizers. Bulk liquid fraction $\ll 1$ vol.%.

(Fig. 8f). At a lower liquid-fraction, the aggregate deforms by grain boundary migration accommodated dislocation creep with welded non-sliding grain boundaries (Fig. 8). The transition between the granular flow regime and the dislocation creep regime is more abrupt between about 6–8 vol.%, compared with the low strain rate experiments, with less development of localized shear zones.

3.2. KNO_3–$LiNO_3$ experiments

In the second type of experiment, the samples were prepared by complete melting of a KNO_3–$LiNO_3$ mixture at 300 °C and subsequent cooling and crystallising between the glass plates, down to 200 °C, at which temperature it was left to anneal for 24 h. At this temperature all $LiNO_3$ is completely molten and the solid phase is only composed of KNO_3 grains. Due to a temperature gradient of about 10 °C between the centre of the observation window (colder) and the metal housing (hot) most of the nitrate melt migrates out of the centre during static grain coarsening (Lesher and Walker, 1988) and collects at the side of the sample, so that the observed area of the sample has a low starting melt fraction of approximately 1 vol.% (Fig. 9a). Because of the low melt fraction and the temperature gradient, the wetting angle is difficult to measure accurately but appears to be well below 60°.

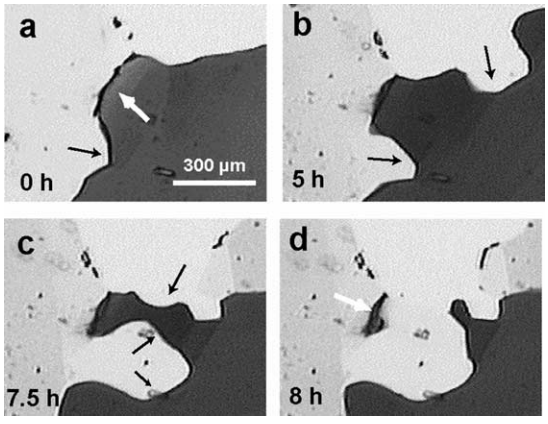

Fig. 7. 'Irregular pinning' in a 'low' strain rate norcamphor+ethanol experiment. The sweeping boundary cannot detach from a larger fluid patch as in Fig. 6. The sides swing around and leave a small island grain connected to a liquid inclusion (see arrows). Images were taken with partly crossed polarizers. Bulk liquid fraction $\ll 1$ vol.%.

Experiments were carried out in pure shear, at a 'high' strain rate of about 10^{-5} s^{-1} and at a constant temperature of 200 °C. At this temperature non-molten $NaNO_3$, a compound similar to KNO_3 in its behaviour, displays rotational recrystallisation and grain boundary migration recrystallisation in the experiments of Tungatt and Humphreys (1981). However, since the KNO_3 grains in our experiments are comparably rigid, deformation is dominated by grain boundary sliding and internal deformation of the grains was only observed at a very low melt fraction <1 vol.% (see below). During progressive deformation small conjugate shear zones develop throughout the sample (Figs. 9–11). Because of the initially low melt fraction the grain boundary sliding depends on a geometrical accommodation process. However, no diffusion or contact melting (cf. Means and Park, 1994) accommodation of the grain boundary sliding was observed but the sliding of grain boundaries was rather accommodated by local dilation and creation of new dynamic porosity in the shear zones. The newly created porosity is filled with melt that is drawn in from the matrix and from the edge of the sample. In this way the segregated melt originally located at the side is redistributed within the sample and the bulk melt fraction of the sample is dynamically increased (Figs. 10 and 12c). Shear zones rotate towards the shear plane and become inactive, as new shear zones develop to take up the strain. The elevated porosity of an inactive shear zone is quickly destroyed by compaction and redistributed into newly formed shear zones (e.g. Fig. 10b and c). As the melt fraction rises during the experiment, the shear zones widen and deformation thereby becomes less localized and progress towards distributed granular flow (e.g. lower left region in Fig. 10d with a local melt fraction $\phi_{local} \approx 9$–10 vol.%). However, this progressive increase in melt fraction is only possible if a sufficiently large melt reservoir is available at the side of the sample that can be sucked into the aggregate during deformation. If the melt fraction cannot increase freely, deformation stays localized in GBS shear zones and the compacting regions are often characterised by a flattening of the crystals, possibly by diffusional creep, or by anomalous fast grain growth (Fig. 11). This stage of framework deformation at which

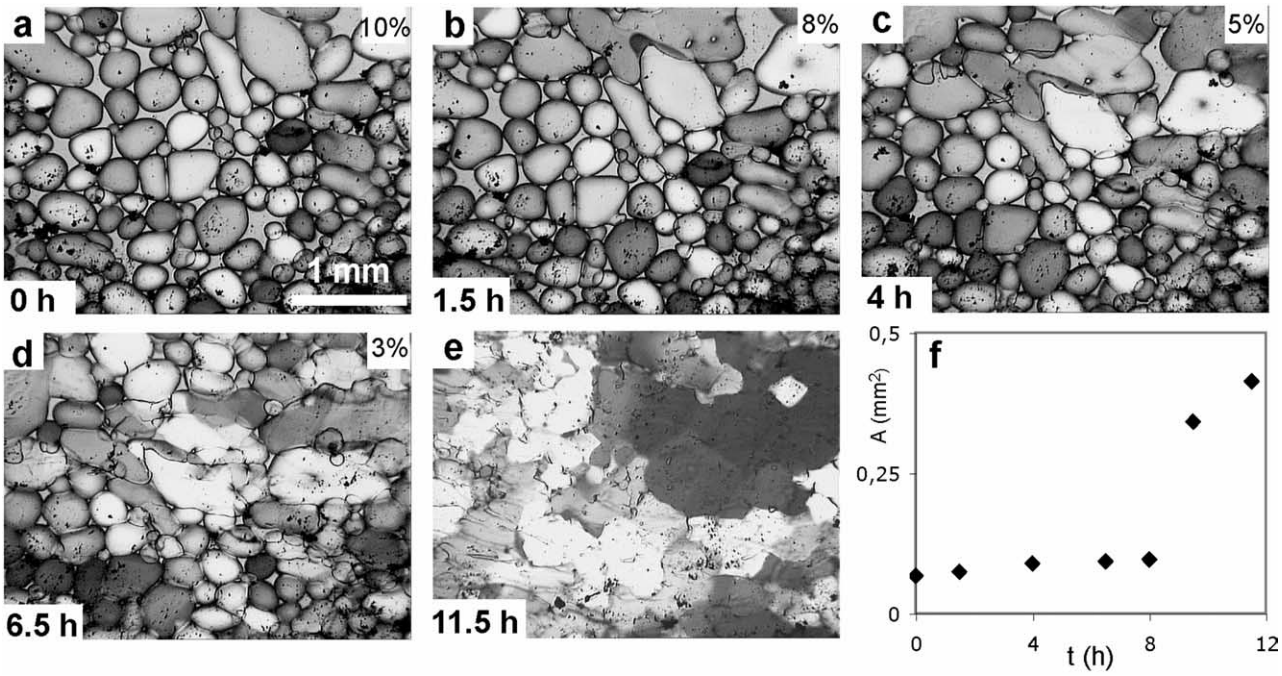

Fig. 8. Deformation of norcamphor crystals plus ethanol liquid by bulk pure shear with a 'high' strain rate of ca. $10^{-5}\,s^{-1}$ (vertical shortening). (a) and (b) Deformation is mainly by grain boundary sliding accommodated compaction. (c) Onset of the locking stage of the grains into one coherent cluster suppressing GBS. Beginning of framework compaction. (d) GBM starts in the liquid-poor central region while liquid pockets still pin the grain boundaries in the other parts. (e) Further compression and liquid removal allows free grain boundary migration. The grain size is now significantly larger than during grain boundary sliding. Images were taken with partly crossed polarizers. Bottom left numbers indicate time elapsed from the beginning of the experiment, top right numbers indicate the liquid fraction in vol.%. (f) Mean grain size versus time graph.

grains lock and the onset of internal crystal plastic deformation is only observed in compacting areas of the samples with a very low melt fraction <1 vol.%. The very low melt fraction for the onset of framework deformation can be explained by the strong grains combined with the low wetting angle of the melt that inhibits grain welding and clustering and favours the formation of dilatant shear zones.

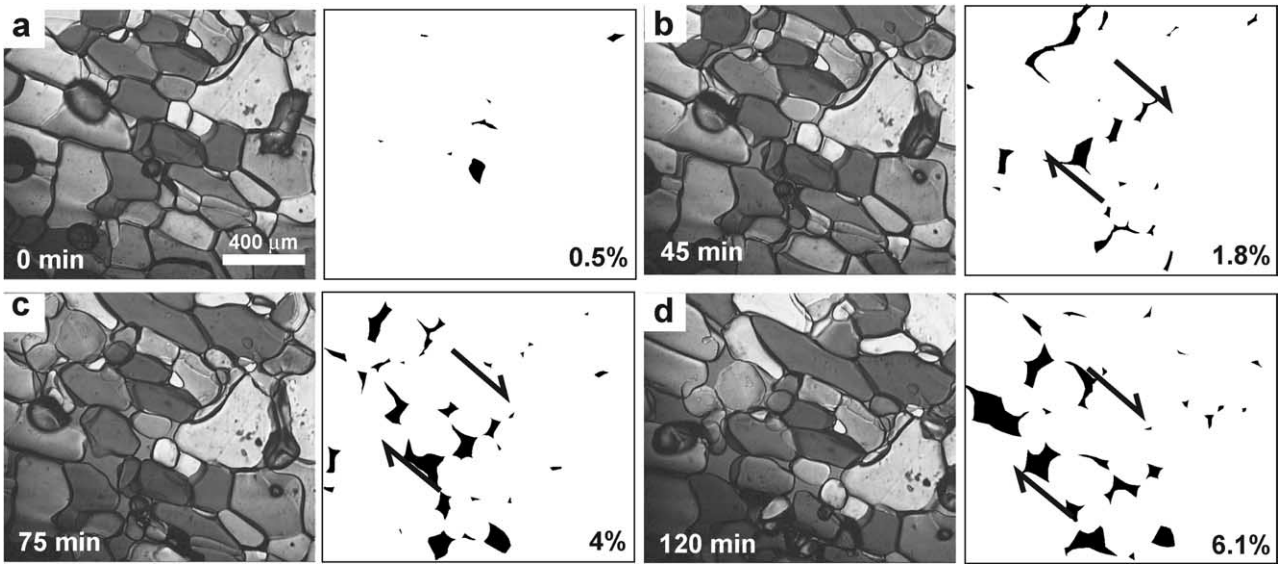

Fig. 9. Nitrate deformation experiment with a bulk pure shear of approximately $10^{-5}\,s^{-1}$ (vertical compression) Binary images trace the liquid evolution, bottom right numbers give the melt vol.%. (a) Potassium nitrate aggregate before deformation with low porosity. (b)–(d) Deformation localizes into a small shear zone that deforms by GBS. Opening gaps are filled with melt that is drawn in from the outside. The dynamic porosity in the shear zone has now significantly increased to approximately 10%, while the matrix has retained a low porosity. Images were taken with partly crossed polarizers. Bottom left numbers indicate time elapsed from the beginning of the experiment.

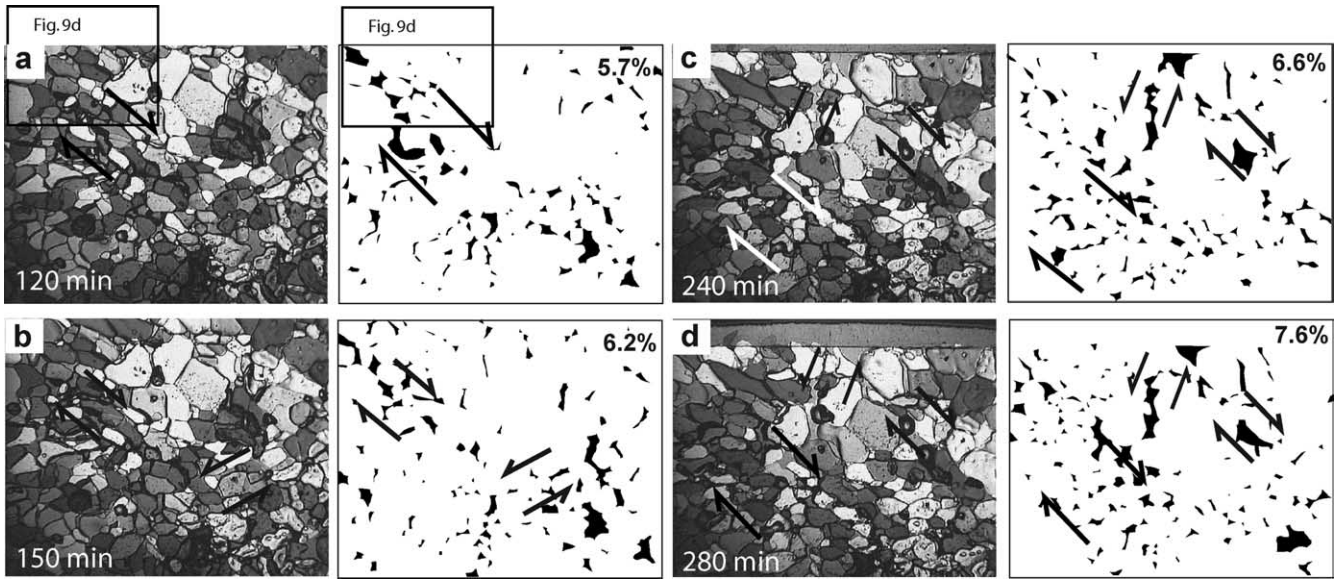

Fig. 10. Nitrate deformation experiment, continued from Fig. 9 with a lower magnification. Observed area of Fig. 9 is marked in (a). Binary images trace the liquid evolution, top right numbers give the melt vol.%. Aggregate deforms by conjugate GBS shear zones. The melt-fraction in the observed area rises during progressive deformation, and the deformation develops from localized shear zones towards distributed granular flow. Bottom left numbers indicate time elapsed from the beginning of the experiment.

3.3. Evolution of the liquid-fraction in the analogue experiments

Fig. 12 shows the evolution of the liquid fraction as a function of the bulk shortening of the norcamphor–ethanol experiments (Fig. 12a and b) and the KNO_3–$LiNO_3$ experiments (Fig. 12c). For the analysis of the norcampor experiments starting images were chosen that contain similar liquid fractions of ~10 vol.% and the shortening was calculated in relation to these starting images. The curves of the low strain rate (Fig. 12a) and the high strain rate (Fig. 12b) experiment show a very similar liquid versus strain evolution in the norcamphor–ethanol system. In the beginning, deformation is dominated by compaction, until at around 8–9 vol.% liquid fraction (10% shortening) the deformation is dominated by liquid assisted granular flow. The subsequent flattening of the liquid curve until a bulk shortening of 30–35% represents temporary inefficient liquid segregation during granular flow. At that stage, below a liquid fraction of ca. 8 vol.%, liquid segregation picks up again when norcamphor grains reach partial locking combined with localized grain boundary sliding (Fig. 12a and b). Although the described departure from linearity of the liquid evolution in Fig. 12 appears not to be very pronounced, it should be noted that it is within measurement precision and that the curve coincides very well with the described microstructural transitions.

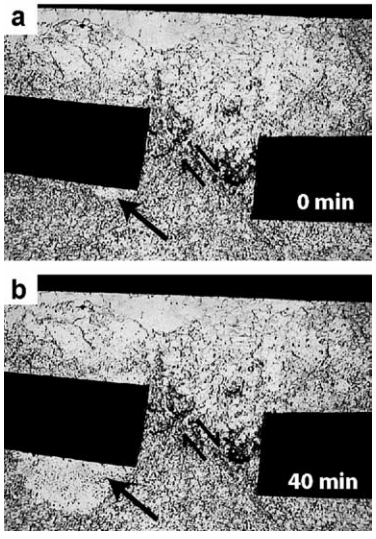

Fig. 11. Nitrate deformation experiment with a low bulk melt fraction (estimated to be <3 vol.%). Black bodies are rigid 'micro boudins' made out of 0.1-mm-thick metal foil. Deformation is by localized GBS with a small shear zone that separates the two 'boudins'. Melt fraction in the shear zone is raised, while the matrix compacts, probably by dislocation creep. Fast, anomalous grain growth (see arrow) overgrows large parts of the fine-grained matrix. Width of view is approximately 1 cm.

The liquid fraction and the microstructural evolution of the nitrate experiments and the norcamphor–ethanol experiments display opposite trends during the experiments. While the latter evolve from high to low liquid-fraction during progressive deformation, the nitrate experiments evolve from low to high liquid-fraction. Thus the norcamphor experiments start with granular flow, which evolves to localized GBS and finally reach framework deformation, while the nitrates start deforming by localized GBS and progress towards granular flow. It is interesting to note that despite these differences the transitions from localized GBS deformation to granular flow is similar for both systems (8–10 vol.%).

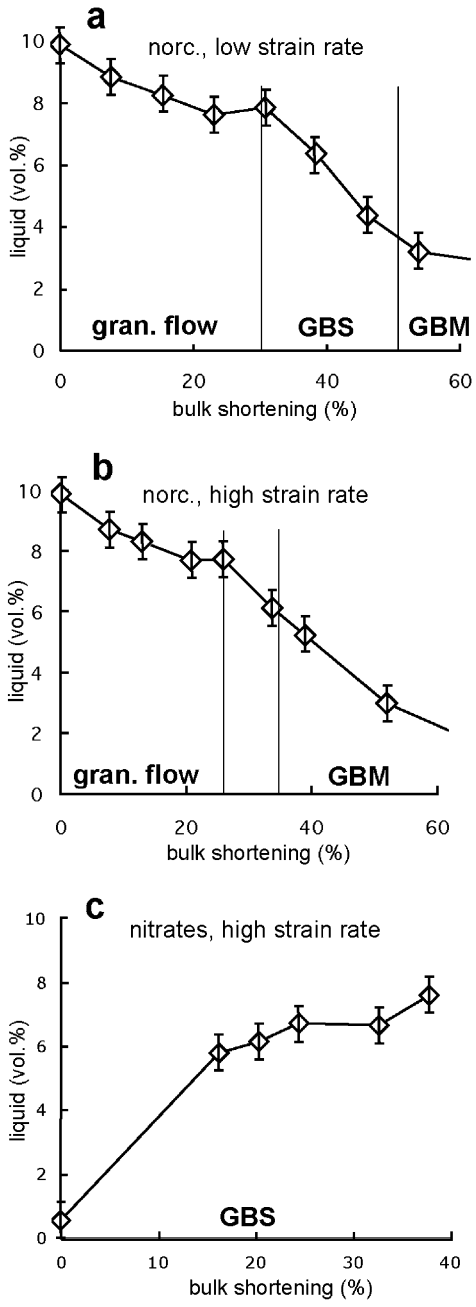

Fig. 12. Evolution of the liquid fraction in the norcamphor–ethanol experiments and the KNO_3-$LiNO_3$ experiment versus bulk strain. (a) Development of the liquid fraction in the low strain rate experiment. Time displayed is 80 h. (b) Liquid evolution in the 'high' strain rate experiment. Approximate positions of microstructural transitions (ϕ_{LT} and $\phi_{GBS\text{-}L}$) are marked with stippled lines. The bulk shortening is calculated in relation to the initial stage at approximately 10% liquid. Time displayed is 5 h. (c) Melt-fraction evolution in the nitrate experiment shown in Figs. 9 and 10.

4. Discussion

The deformation behaviour of all described analogue systems can be classified into three deformation regimes: at a 'high' liquid-fraction ($\phi_{bulk} \geq 8$–10 vol.%) deformation is by compaction and distributed granular flow (regime I), at a 'moderate' liquid-fraction ($\phi_{bulk} < 8$–10 vol.%) deformation is by localized GBS with compacting grain clusters in between (regime II), and at a 'low' liquid-fraction (ϕ_{bulk} varies depending on the system) an interlocking granular framework is deformed (regime III). The following sections discuss the implications of these observations for the deformation behaviour of partially-molten rocks and for the small-scale distribution of liquid in general.

4.1. Deformation regime I (granular flow) and regime II (localized grain boundary sliding)

The term grain boundary sliding (GBS) is used here to characterize the grain-scale deformation mechanism of grains moving relative to each other. The experiments have shown that GBS is the dominant deformation mechanism at a high to moderate liquid fraction above about 4–6 vol.% in the norcamphor–ethanol experiments and above ca. 1 vol.% in the KNO_3–$LiNO_3$ experiments. GBS-dominated deformation behaviour was subdivided into two regimes based on the degree of strain localization. If deformation is distributed throughout the aggregate without or with only minor strain localization, we use the term granular flow (deformation regime I). Granular flow was observed in both sets of analogue experiments and in the analogue experiments of Park and Means (1996) at a liquid fraction of ≥ 8–10 vol.%. At a lower liquid fraction GBS deformation is localized in shear zones in our experiments, which we call localized GBS (deformation regime II).

Granular flow and grain boundary sliding of partially-molten rocks is considered as a potentially important deformation mechanism in nature (e.g. Rutter, 1997; Paterson, 2001; Rosenberg, 2001; Mecklenburgh and Rutter, 2003). Theoretical models for GBS consider diffusional creep and reactions as rate limiting parameters and therefore predict Newtonian flow behaviour (Paterson, 2001). However, experimental investigations generally result in a higher strain rate sensitivity, such as $n \approx 3.5$ for quartz plus albite–quartz melt (Rutter and Neumann, 1995; Mecklenburgh and Rutter, 2003). This power-law behaviour indicates that another mechanism than diffusion is rate controlling. Mecklenburgh and Rutter (2003) suggested fracturing and intra-grain microcracking for higher strain rates and the destruction of welded grain boundaries (inter-grain microfracturing) for low strain rates as alternative mechanisms. The latter process is also observed in our experiments. In our norcamphor–ethanol experiments, grain boundaries are continuously welded and separated (Fig. 4). Although the opening of welded grain boundaries may be the rate-controlling mechanism for GBS deformation, a freely moving liquid is required to provide the geometric porosity for grains to slide past each other. This process is evident from our experiments and explains the degree of deformation localization observed. At a bulk liquid fraction ≥ 8–10 vol.% GBS deformation can occur as non-localized granular flow (deformation regime I). At a lower liquid

fraction there is insufficient liquid to let the whole aggregate deform by GBS and deformation is localized into GBS shear zones (regime II, e.g. Fig. 10). Similar relatively melt-enriched shear zones have been observed in olivine- and feldspar-melt deformation experiments (Holtzman et al., 2003a,b) and in norcamphor–benzamide analogue experiments (Rosenberg and Handy, 2000).

Natural examples of regime II behaviour could be the small melt-filled shear zones or shear bands that are frequently observed in natural partially molten rocks (e.g. Brown, 1994; Brown and Rushmer, 1997; Brown and Solar, 1998). Brown and Rushmer (1997) proposed melt-induced local fracturing and cataclastic flow to explain the increased porosity. Alternatively, if the systems deformed in regime II, small initial melt fraction fluctuations would naturally cause small shear zones with a raised melt fraction that deform by GBS.

4.2. The localization threshold (ϕ_{LT})

Because of the importance of the liquid fraction for determining the localization of GBS deformation, we suggest calling the liquid fraction that separates regime I from regime II the localization threshold (ϕ_{LT}). If the bulk liquid fraction of a liquid-bearing aggregate exceeds ϕ_{LT} for a given system ($\phi_{bulk} > \phi_{LT}$), flow is by pervasively distributed granular flow with or without compaction (regime I, Fig. 13a). If the bulk liquid fraction is lower than ϕ_{LT} ($\phi_{bulk} < \phi_{LT}$), GBS shear zones with a locally raised liquid fraction are formed (regime II, Fig. 13b). ϕ_{LT} is a transition zone at about 8–10 vol.% in the case of two-dimensional (2-D) analogue experiments. In three-dimensional (3-D) reality, ϕ_{LT} is expected to be higher, probably around 25–30 vol.%. This can be derived from comparing the pore area fraction of a closest circle packing in 2-D to the pore volume fraction of closest sphere packing in 3-D, which is ca. 9 and 26 vol.%, respectively.

4.3. Deformation regime III: grain boundary migration accommodated dislocation creep

Deformation regime III is characterized by the welding of all grain boundaries into a coherent cluster at a liquid fraction below ca. 4–7 vol.% in the norcamphor–ethanol

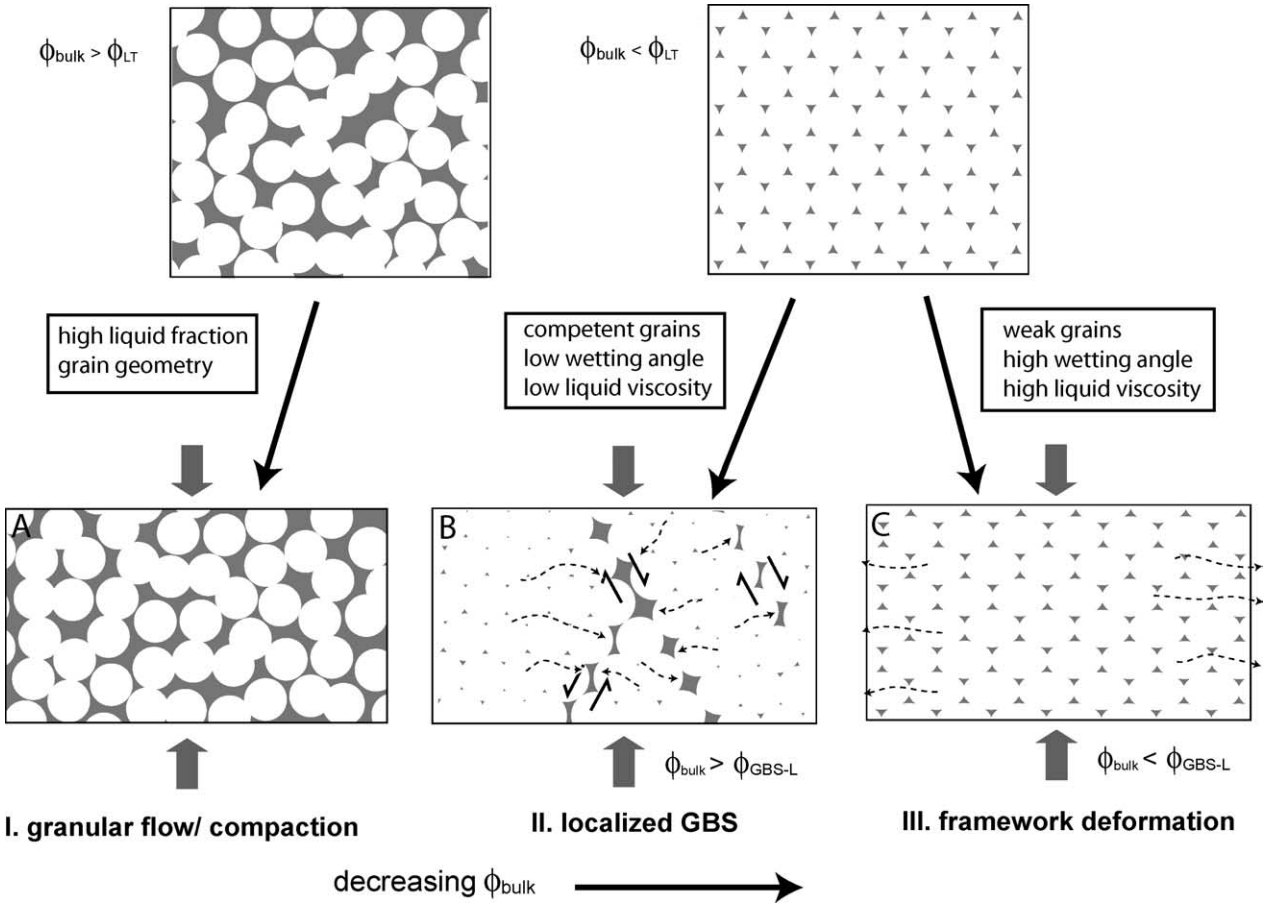

Fig. 13. Schematic representation of the observed deformation regimes. (a) At high liquid fraction ($\phi_{bulk} > \phi_{LT}$) a solid–liquid aggregate deforms by compaction and granular flow (regime I). At a lower liquid fraction ($\phi_{bulk} < \phi_{LT}$) a solid–liquid aggregate can either deform by localized grain boundary sliding (b) (regime II, $\phi_{bulk} > \phi_{GBS\text{-}L}$) or by framework deformation (c) (regime III, $\phi_{bulk} > \phi_{GBS\text{-}L}$). Note that knowledge of the initial microstructure and liquid fraction is not sufficient for determining the deformation regime.

experiments and below about 1 vol.% in the nitrate experiments. A common observation from both sets of experiments was the anomalous grain growth, which occurred during framework deformation and led to a significant increase of the grain size. This increase of grain size during deformation appears to be different from previously described processes of abnormal or discontinuous grain growth (cf. Atkinson, 1988; Evans et al., 2001, and references therein) or exaggerated grain growth (cf. Vernon, 1976), in which single larger grains grow at the expense of smaller matrix grains, since the latter occurred during static recrystallisation.

The microstructures observed during grain boundary migration in the norcamphor experiments correspond to the dislocation creep regime 3 of Hirth and Tullis (1992) and the GBM regime of Stipp et al. (2002a,b) that are characterized by grain boundary migration accommodated dislocation creep with only minor sub-grain rotation recrystallisation. Although these regimes have been defined for non-molten deforming quartzite, our observation that the strong grain boundary migration only starts when nearly all melt has been removed from the sample fits well with the description of regime 3, especially since a very low melt fraction $<1\%$ was reported for some of the experiments of Hirth and Tullis (1992). However, the very high mobility of the grain boundaries and the dramatic increase of the grain size in our experiments are unusual for the unmolten GBM regime of Hirth and Tullis (1992). The sudden grain growth that was observed in some of the nitrate experiments (e.g. Fig. 11) was even more pronounced than in the norcamphor experiments. This grain size increase is probably the result of a similar process as in the norcamphor, since the temperature of deformation (200 °C) in our experiments lies within the range of GBM recrystallisation in $NaNO_3$ reported by Tungatt and Humphreys (1981).

Liquid-enhanced grain boundary mobility has been reported in other materials, such as wet bischofite (Urai, 1983) and norcamphor plus norcamphor–benzamide melt (Rosenberg and Handy, 2001). In a natural example, Stipp et al. (2002b) reported an unexplained dramatic increase in grain size of a deformed quartzite adjacent to the contact of the Adamello pluton (Italian Alps). Although the quartzite layers do not contain visible traces of melt, the pluton and the surrounding rocks were partially molten during the deformation (Stipp, personal communication, 2004). It is therefore possible that small traces of melt were present in the quartzite layers during deformation, which lead to a similar dynamic grain-size increase, as observed in our experiments. A very large grain size is also a characteristic of high-temperature quartz ribbon mylonites (e.g. Hippert et al., 2001), which could similarly be connected to the presence of a low percentage of melt or metamorphic fluid during crystal plastic deformation. The results of our analogue experiments and of the examples given above indicate that while macroscopic liquid or melt pockets tend to inhibit grain boundary mobility by pinning (Figs. 6 and 7), a very low liquid fraction might enhance grain boundary mobility. Similar conclusions were drawn by Renner et al. (2002) for static systems.

4.4. The grain boundary sliding–grain boundary locking (GBS-L) transition

Below ϕ_{LT} there is a second transition ($\phi_{GBS\text{-}L}$) from (localized) grain boundary sliding to crystal–plastic framework deformation, when the framework gets locked. Unlike ϕ_{LT}, $\phi_{GBS\text{-}L}$ is sharp in our experiments.

A critical question for the GBS-L transition concerns the conditions under which a locked framework is established that can support the applied stress without or with only minor grain-boundary sliding. To better characterize the magnitude and variation of $\phi_{GBS\text{-}L}$ for different systems, we have to consider the parameters of our analogue experiments that determine and influence $\phi_{GBS\text{-}L}$. In the norcamphor–ethanol GBS regime spontaneous welding and clustering between adjacent norcamphor grains is energetically favourable and might act as a rate limiting mechanism for GBS deformation as discussed in Section 4.1. Thus, the total work necessary for continuous grain boundary sliding in addition to overcoming frictional forces is the work necessary to locally break one solid–solid grain boundary times the total number of boundaries. The number of welded grain boundaries and the ratio of the solid–solid to solid–liquid boundary area in a sample directly depend on the liquid fraction, so that the work per strain increment of GBS increases with decreasing liquid fraction. Thus, $\phi_{GBS\text{-}L}$ occurs at that liquid fraction at which the strain energy rate for maintaining GBS equals or exceeds the strain energy rate for framework deformation. Several parameters should influence the magnitude of $\phi_{GBS\text{-}L}$ (see also Fig. 13):

1. *Solid strength and liquid viscosity*: A strong solid phase with a relatively low viscosity liquid facilitates GBS and therefore lowers $\phi_{GBS\text{-}L}$ (e.g. nitrate experiments), compared with a system with a weaker solid phase with a relatively higher viscosity liquid which facilitates framework deformation and thereby raises $\phi_{GBS\text{-}L}$ (e.g. norcamphor experiments). The solid–liquid viscosity ratio can change in a system as a function of strain rate (the strain rate sensitivity) and temperature, thereby changing $\phi_{GBS\text{-}L}$.
2. *The bonding strength of grain boundaries*: This is probably a function of the solid–solid surface energy, the wetting angle, and the relative liquid pressure. A well-wetting liquid will facilitate dynamic wetting and breaking of grain boundaries so that $\phi_{GBS\text{-}L}$ is lowered compared with a similar system with a poorly-wetting liquid. Furthermore, the relative liquid pressure is of importance for breaking of grain boundaries and creating dynamic porosity. Liquid overpressure facilitates breaking of grain boundaries, thereby lowering $\phi_{GBS\text{-}L}$.

3. *Grain size*: In grain-size sensitive framework deformation (liquid-assisted diffusional creep), $\phi_{GBS\text{-}L}$ is raised by a decreasing grain size.
4. *Permeability and viscosity*: To create localized shear zones, liquid has to move a certain distance along a hydraulic head into the shear zones. This migration from the matrix into the shear zones is a function of liquid viscosity and matrix permeability (see Holtzman et al., 2003a).

4.5. Relation to other threshold models (RCMP, RPT, PLT)

Arzi (1978) suggested the existence of a rheological critical melt percentage (RCMP), which marks a transition between essentially solid behaviour to much weaker melt-dominated behaviour. The RCMP concept predicts a sharp drop in strength at a bulk melt fraction of about $\phi_{bulk} \approx 20 \pm 10\%$ melt. Vigneresse et al. (1996) and Vigneresse and Tikoff (1999) extended and modified the concept by arguing that there is a difference between a progressively melting system (increasing melt fraction) and a crystallising system (decreasing melt fraction) and defined four thresholds by utilizing percolation theory. In the crystallising case they defined the rigid percolation threshold (RPT) at $\phi_{bulk} \approx 45$ vol.% and the particle locking threshold (PLT) at $\phi_{bulk} \approx 25$–28 vol.%. The PLT is analogous to the RCMP. All authors have in common that they base their theory on the consideration that once a geometric stress-supporting framework of rigid grains has been established, the rheology of the system should change dramatically. The melt fraction at the transition between solid- and liquid-dominated behaviour is argued to depend mainly on the particle shape.

Although the existence of a RCMP is not undisputed (e.g. Bagdasserov and Dorfman, 1998; Renner et al., 2000; Rosenberg, 2001), our observations, and those of Park and Means (1996), support a microstructural transition from liquid-dominated (regimes I–II) to framework-dominated (regime III) behaviour, comparable with the rheological RCMP. Whereas previous authors (Vigneresse et al., 1996; Vigneresse and Tikoff, 1999) set the RCMP exactly at the liquid fraction where the solid phase forms a connecting framework, we show that redistribution of the liquid may significantly lower the transition to regime III behaviour.

An indication of the transition from regime II to III ($\phi_{GBS\text{-}L}$) in nature may be derived from the careful mapping of grain-scale melt pseudomorphs in migmatites that was presented by Sawyer (2001). His fig. 2 (p. 294) shows an elongate melt-enriched zone, with about 25 vol.% melt, in a matrix with only 6–13 vol.% melt. The microstructure, with a bulk melt fraction about 12.5 vol.% melt, is similar to our regime II, suggesting that $\phi_{GBS\text{-}L}$ lies below 12.5 vol.% in this partially molten pelite.

4.6. Segregation of liquid

Efficient melt segregation at melt fractions above the RCMP is predicted to occur by compaction and filter pressing, whereas only restricted segregation occurs below the RCMP once a solid framework is established (Arzi, 1978). Interestingly, our results indicate the opposite. The liquid-fraction evolution of the experiments show that segregation of liquid per strain increment is significantly slower or even reversed (in the nitrate experiments) during granular flow and grain-boundary sliding (regimes I–II), while liquid segregation is most efficient during regime III framework deformation (Fig. 12). The reason is that grain boundary sliding can only occur with a sufficient liquid fraction (ϕ_{GSP}) and local dilation and compaction will shuffle liquid around, rather than expel it. Efficient filter pressing can only occur in regime III where the deforming framework can effectively exert a pressure on the low-viscous liquid to expel it to any available sinks.

5. Conclusions

Experiments performed with the liquid-bearing norcamphor–ethanol system and the partially molten KNO_3–$LiNO_3$ system give information on a range of deformation mechanisms that potentially act in partially molten and fluid-bearing rocks from high to very low liquid fractions. The deformation behaviour of the analogue systems is characterised by three different deformation regimes (quoted liquid fractions are for 2-D experiments, and are probably higher for 3-D systems).

5.1. 'High' liquid fraction $\geq$8–10 vol.%: compaction and granular flow

At liquid fraction $>10\%$ deformation is dominated by compaction. Strain is accommodated by grain rearrangement, GBS, and, at sufficiently low strain rate, by the disappearance of small grains due to grain coarsening whose space is taken up by larger grains. At a liquid fraction of about 8–10 vol.% (ϕ_{LT}) deformation of the norcamphor–ethanol and the KNO_3–$LiNO_3$ experiments is by distributed granular flow. In the norcamphor–ethanol experiments, liquid segregation is least efficient at liquid fractions just above ϕ_{LT}. In the KNO_3–$LiNO_3$ experiments, liquid segregation is even reversed by drawing in melt to enable GBS.

5.2. 'Moderate' liquid fraction: localized grain boundary sliding

Below 8–10 vol.% (ϕ_{LT}) the 'low' strain rate norcamphor–ethanol experiments and the nitrate experiments often exhibit conjugate shear zones that deform by GBS. The areas in between form grain clusters that compact slightly

and thereby loose liquid to the shear zones ($\phi_{local} < \phi_{bulk}$) or to the edge of the sample, while the liquid fraction in the shear zones increases ($\phi_{local} \approx \phi_{LT} > \phi_{bulk}$). The degree of localisation increases with a decreasing liquid fraction. The 'high' strain rate norcamphor experiments exhibit this deformation stage to a lesser degree but progress more directly from regime I to regime III.

5.3. 'Low' liquid fraction: framework deformation by dislocation creep

The grains of the solid–liquid systems form a stress-supporting framework that deforms internally by a mechanism of framework deformation such as dynamic recrystallisation accommodated dislocation creep (norcamphor–ethanol experiments). The grains recrystallise by very mobile grain boundaries that sweep highly strained areas of other crystals. Rotational recrystallisation takes place with initial undulouse extinction that concentrates into sub-grain boundaries, and finally the formation of new grains. These structures are similar to high-temperature deformation regime 3 in Hirth and Tullis (1992) and GBM regime of Stipp et al. (2002). The nitrate system exhibits anomalous grain growth.

In our experiments, GBS deformation is not accommodated by diffusion creep as generally assumed (e.g. Paterson, 2001), but by the continuous destruction of grain boundaries and by an increased dynamic porosity through the influx of liquid into the deforming region. This requires that the liquid fraction locally exceeds a localization threshold (ϕ_{LT}) that depends on the grain geometry. If $\phi_{bulk} \geq \phi_{LT}$ all systems deform by granular flow and thereby completely loose cohesion. Since ϕ_{LT} is a geometric threshold, it can be expected to be similar in all solid–liquid systems with approximately equant crystals (8–10 vol.% in 'two-dimensional' experiments). The transition between regimes II and III is called the grain boundary sliding–grain boundary locking threshold ($\phi_{GBS\text{-}L}$). In contrast to ϕ_{LT}, $\phi_{GBS\text{-}L}$ varies depending on several parameters such as strain rate, strength of the grains and the strength of welded grain boundaries. In our experiments, $\phi_{GBS\text{-}L}$ varied between ca. 7–6 vol.% (high strain rate norcamphor–ethanol experiment) and ca. 1% (KNO_3–$LiNO_3$ experiments). Earlier threshold models (e.g. the RCMP; Arzi, 1978) considered the geometric formation of a stress-supporting framework to represent the main rheological switch in liquid-bearing systems. The existence of deformation regime II has the consequence that a system with a liquid fraction that would geometrically allow the formation of a stress (strain) supporting framework ($\phi_{bulk} < \phi_{LT}$) can 'avoid' framework deformation by redistributing the liquid into GBS shear zones. Examples for this process could be migmatites and melt-bearing HT experiments that display strain and melt localization into small shear zones or shear bands.

Acknowledgements

We thank Daniel Koehn, Marlina Elburg, and Jochen Arnold for help and fruitful discussions. The reviewers J. Tullis and E. Rutter are thanked for constructive reviews that helped to improve and clarify the manuscript. N. Walte acknowledges funding by the DFG-Graduiertenkolleg 'Composition and Evolution of Crust and Mantle'.

References

Arnold, J., Jacoby, W.R., Schmeling, H., Schott, B., 2001. Continental collision and the dynamic and thermal evolution of the Variscan orogeniccrustal root—numerical models. Journal of Geodynamics 31, 273–291.

Arzi, A.A., 1978. Critical phenomena in the rheology of partially melted rocks. Tectonophysics 44, 173–184.

Atkinson, H.V., 1988. Overview no. 65: theories of normal grain growth in pure single phase systems. Acta Metallica 36, 469–492.

Bagdasserov, N., Dorfman, A., 1998. Granite rheology: magma flow and melt migration. Journal of the Geological Society London 155, 863–872.

Barcilon, V., Richter, F.M., 1986. Non-linear waves in compacting media. Journal of Fluid Mechanics 164, 429–448.

Bauer, P., Rosenberg, C., Handy, M.R., 2000. 'See-through' deformation experiments on brittle-viscous norcamphor at controlled temperature, strain rate and applied confining pressure. Journal of Structural Geology 22, 281–289.

Bons, P.D., 1993. Experimental deformation of polyphase rock analogues. Geologica Ultraiectina 110, Utrecht.

Bons, P.D., Jessell, M.W., Passchier, C.W., 1993. The analysis of progressive deformation from dispersed marker-particles. Journal of Structural Geology 15, 403–411.

Brown, M., 1994. The generation, segregation, ascent and emplacement of granite magma: the migmatite-to-crustally-derived granite connection in thickened orogens. Earth-Science Reviews 36, 83–130.

Brown, M., Rushmer, T., 1997. The role of deformation in the movement of granitic melt: views from the laboratory and the field. In: Holness, M.B. (Ed.), Deformation Enhanced Fluid Transport in the Earth's Crust and Mantle The Mineralogical Society Series, vol. 8. Chapman and Hall, London, pp. 111–144.

Brown, M., Solar, G., 1998. Shear-zone systems and melts: feedback relations and self-organization in orogenic belts. Journal of Structural Geology 20, 211–227.

Dell'Angelo, L.N., Tullis, J., 1988. Experimental deformation of partially melted granitic aggregates. Journal of Metamorphic Geology 6, 495–515.

Einstein, A., 1906. Eine neue Bestimmung der Moleküldimensionen. Annalen der Physik 19, 289–306.

Evans, B., Renner, J., Hirth, G., 2001. A few remarks on the kinetics of static grain growth in rocks. International Journal of Earth Science 90, 88–103.

Gleason, G.C., Bruce, V., Green, H.W., 1999. Experimental investigation of melt topology in partially molten quartzo-feldspathic aggregates under hydrostatic and non-hydrostatic stress. Journal of Metamorphic Geology 17, 705–722.

Herweg, M., Handy, M.R., 1996. The evolution of high-temperature mylonitic microfabrics: evidence from simple shearing of a quartz analogue (norcamphor). Journal of Structural Geology 18, 689–710.

Hippert, J., Rocha, A., Lana, C., Egydio-Silva, M., Takeshita, T., 2001. Quartz plastic segregation and ribbon development in high-grade striped gneisses. Journal of Structural Geology 23, 67–80.

Hirth, G., Kohlstedt, D.L., 1995a. Experimental constrains on the dynamics of the partially molten upper mantle: deformation in the diffusion creep regime. Journal of Geophysical Research 100, 1981–2001.

Hirth, G., Kohlstedt, D.L., 1995b. Experimental constrains on the dynamics of the partially molten upper mantle: deformation in the dislocation creep regime. Journal of Geophysical Research 100, 15441–15449.

Hirth, G., Tullis, J., 1992. Dislocation creep regimes in quartz aggregates. Journal of Structural Geology 14, 145–159.

Holtzman, B.K., Groebner, N.J., Zimmerman, M.E., Ginsberg, S.B., Kohlstedt, D.L., 2003a. Stress-driven melt segregation in partially molten rocks. Geochemistry, Geophysics, Geosystems 4, 8607. doi:10.1029/2001GC000258.

Holtzman, B.K., Kohlstedt, D.L., Zimmerman, M.E., Heidelbach, F., Hiraga, T., Hustoft, J., 2003b. Melt segregation and strain partitioning: implications for seismic anisotropy and mantle flow. Science 103, 1227–1230.

Holyoke, C.W., Rushmer, T., 2002. An experimental study of grain scale melt segregation mechanisms in two common crustal rock types. Journal of metamorphic Geology 20, 493–512.

Jurewicz, S.R., Watson, E.B., 1985. The distribution of partial melt in a granitic system; the application of liquid phase sintering theory. Geochimica et Cosmochimica Acta 49 (5), 1109–1121.

Kelemen, P.B., Hirth, G., Shimizu, N., Spiegelman, M., Dick, H.J.B., 1997. A review of melt migration processes in the asthenospheric mantle beneath oceanic spreading centers. Philosophical Transactions of the Royal Society London 355, 283–318.

Laporte, D., 1994. Wetting behaviour of partial melts during crustal anatexis: the distribution of hydrous silicic melts in polycrystalline aggregates of quartz. Contibutions to Mineralogy and Petrology 116, 486–499.

Lesher, C.E., Walker, D., 1988. Cumulate maturation and melt migration in a temperature gradient. Journal of Geophysical Research 93, 10295–10311.

McMcKenzie, D., 1987. The compaction of igneous and sedimentary rocks. Journal of the Geological Society, London 144, 299–307.

Means, W.D., 1989. Synkinematic microscopy of transparent polycrystals. Journal of Structural Geology 11, 163–174.

Means, W.D., Park, Y., 1994. New experimental approach to understanding igneous texture. Geology 22, 323–326.

Mecklenburgh, J., Rutter, E.H., 2003. On the rheology of partially molten synthetic granite. Journal of Structural Geology 25, 1575–1585.

Mei, S., Bai, W., Hiraga, T., Kohlstedt, D.L., 2002. Influence of melt on the creep behaviour of olivine-basalt aggregates under hydrous conditions. Earth and Planetary Science Letters 201, 491–507.

van der Molen, I., Paterson, M.S., 1979. Experimental deformation of partially-melted granite. Contributions to Mineralogy and Petrology 70, 299–318.

Park, Y., Means, W.D., 1996. Direct observation of deformation processes in crystal mushes. Journal of Structural Geology 18, 847–858.

Paterson, M.S., 2001. A granular flow theory for the deformation of partially molten rock. Tectonophysics 335, 51–61.

Paterson, S.R., Vernon, R.H., 1995. Bursting the bubble of ballooning plutons: a return to nested diapirs emplaced by multiple processes. Geological Society of America Bulletin 107, 1356–1380.

Petford, N., Koenders, M.A., 1998. Granular flow and viscous fluctuations in low Bagnold number granitic magmas. Journal of the Geological Society, London 155, 873–881.

Rabinowicz, M., Genthon, P., Ceuleneer, G., Hillairet, M., 2001. Compaction in a mantle mush with high melt concentrations and the generation of magma chambers. Earth and Planetary Science Letters 188, 313–328.

Renner, J., Evans, B., Hirth, G., 2000. On the rheological critical melt fraction. Earth and Planetary Science Letters 181, 585–594.

Renner, J., Evans, B., Hirth, G., 2002. Grain growth and inclusion formation in partially molten carbonate rocks. Contributions to Mineralogy and Petrology 142, 501–514.

Rosenberg, C.L., 2001. Deformation of partially molten granite; a review and comparison of experimental and natural case studies. In: Dresen, G., Handy, M. (Eds.), Deformation Mechanisms, Rheology and Microstructures International Journal of Earth Sciences, vol. 90, p. 60.

Rosenberg, C.L., Handy, M.R., 2000. Syntectonic melt pathways during simple shearing of a partially molten rock analogue (norcamphor–benzamide). Journal of Geophysical Research 105, 3135–3149.

Rosenberg, C.L., Handy, M.R., 2001. Mechanisms and orientation of melt segregation paths during pure shearing of a partially molten rock analog (norcamphor–benzamide). Journal of Structural Geology 23, 1917–1932.

Rutter, E.H., 1997. The influence of deformation on the extraction of crustal melts: a consideration of the role of melt-assisted granular flow. In: Holness, M.B. (Ed.), Deformation Enhanced Fluid Transport in the Earth's Crust and Mantle. The Mineralogical Society Series, vol. 8. Chapman and Hall, London, pp. 82–110.

Rutter, E.H., Neumann, D.H.K., 1995. Experimental deformation of partially molten westerly granite under fluid-absent conditions, with implications for the extraction of granitic magmas. Journal of Geophysical Research 100, 15697–15715.

Ryerson, F.J., Weed, H.C., Piwinskii, A.J., 1988. Rheology of subliquidus magmas 1. Picritic compositions. Journal of Geophysical Research 93, 3421–3436.

Sawyer, E., 2001. Melt segregation in the continental crust: distribution and movement of melt in anatectic rocks. Journal of Metamorphic Geology 19, 291–309.

Schott, B., Schmeling, H., 1998. Delamination and detachment of a lithospheric root. Tectonophysics 296, 225–247.

Scott, D., Stevenson, D., 1986. Magma ascent by porous flow. Journal of Geophysical Research 91, 9283–9296.

Stephenson, I.M., White, J., 1967. Factors controlling microstructure and grain growth in two-phase (one solid + one liquid) and in three-phase (two solid + one liquid) systems. Transactions of the British Ceramic Society 66, 443–483.

Stipp, M., Stünitz, H., Heilbronner, R., Schmid, S.M., 2002a. Dynamic recrystallization of quartz; correlation between natural and experimental conditions. In: de Meer, S., Drury, M.R., de Bresser, J.H.P., Pennock, G.M. (Eds.), Deformation Mechanisms, Rheology and Tectonics; Current Status and Future Perspectives Geological Society Special Publications, vol. 200, pp. 171–190.

Stipp, M., Stünitz, H., Heilbronner, R., Schmid, S., 2002b. The eastern tonalite fault zone: a 'natural laboratory' for crystal plastic deformation of quartz over a temperature range from 250 to 700 °C. Journal of Structural Geology 24, 1861–1884.

Tungatt, P.D., Humphreys, F.J., 1981. An in situ optical investigation of the deformation behaviour of sodium nitrate, an analogue for calcite. In: Lister, G.S., Behr, H.J., Weber, K., Zwart, J.J. (Eds.), The Effect of Deformation on Rocks. Tectonophysics, vol. 78, pp. 661–675.

Urai, J.L., 1983. Deformation of wet salt rocks: an investigation into the interaction between mechanical properties and microstructural processes during deformation of polycrystalline carnallite and bischofite in the presence of a pore fluid. PhD thesis, University of Utrecht.

Vernon, R.H., 1976. Metamorphic Processes. Reactions and Microstructure Development. George Allen & Unwin Ltd, London. 247pp.

Vigneresse, J.L., Tikoff, B., 1999. Strain partitioning during melting and crystallizing felsic magmas. Tectonophysics 312, 117–132.

Vigneresse, J.L., Barbey, P., Cuney, M., 1996. Rheological transitions during partial melting and crystallization with application to felsic magma segregation and transfer. Journal of Petrology 37, 1579–1600.

von Bargen, N., Waff, H., 1986. Permeabilities, interfacial areas and curvatures of partially molten systems: results of numerical computations of equilibrium microstructures. Journal of Geophysical Research 91, 9261–9276.

Walte, N.P., Bons, P.D., Passchier, C.W., Koehn, D., 2003. Disequilibrium melt distribution during static recrystallization. Geology 31, 1009–1012.

Weinberg, R.F., Podladchikov, Y.Y., 1994. Diapiric ascent of magmas through power law crust and mantle. Journal of Geophysical Research 99, 9543–9559.